Impurity effects on atomic bonding in Ni_3Al

Sheng N. Sun, Nicholas Kioussis, and Say-Peng Lim
Department of Physics and Astronomy, California State University, Northridge, California 91330

A. Gonis and William H. Gourdin
Lawrence Livermore National Laboratory, Department of Chemistry and Material Science, Livermore, California 94551
(Received 24 March 1995; revised manuscript received 31 July 1995)

First-principles electronic structure calculations based on the full-potential linear-muffin-tin-orbital method have been employed to study the contrasting effects of boron and hydrogen on the electronic structure of the $L1_2$ ordered intermetallic Ni_3Al. The total energy, the site- and l-projected densities of states, and the impurity-induced charge-density characteristics are calculated for various impurity configurations, to investigate the effects of local environment on the electronic structure. Total-energy calculations show that both boron and hydrogen impurities prefer to occupy octahedral interstitial sites that are entirely coordinated by six nickel atoms. Our results suggest that the underlying mechanism of the boron-induced strengthening in Ni_3Al is the Ni-d and B-p hybridization between the nearest-neighbor nickel and boron sites. This results in an enhancement of the intraplanar metallic bonding between the nickel atoms, an enhancement of interstitial bonding charge, and reduction of the bonding-charge directionality around the Ni atoms on the (001) NiAl planes. In contrast, hydrogen is found to enhance the bonding-charge directionality near some Ni atoms and to reduce the interstitial charge, suggesting that it promotes poor local cohesion. When both boron and hydrogen are present in Ni_3Al, the dominant changes in the electronic structure are induced by boron and the charge distribution resembles that of Ni_3Al+B. These results are broadly consistent with the notion of boron as a cohesion enhancer and hydrogen as an embrittler.

I. INTRODUCTION

The past two decades have witnessed dramatic growth in both experimental and theoretical activity in intermetallic compounds and ordered alloys, because of their potential use in a wide variety of technological applications.[1] Among the intermetallic compounds, the $L1_2$-type ordered nickel aluminide Ni_3Al exhibits unique mechanical properties that make it attractive for structural applications at elevated temperatures. Of central interest are its high melting temperature, low density, resistance to oxidation,[2] and the increase of yield stress it displays with increasing temperature,[3] in contrast to conventional compounds or disordered alloys. However, as with many other intermetallics, an inherent drawback to using Ni_3Al as a structural material is the tendency of polycrystalline ordered stoichiometric alloys to undergo brittle intergranular fracture,[4] even though single crystals of Ni_3Al are highly ductile.

Microalloying studies have shown[2] that doping with certain impurities, which strongly segregate toward grain boundaries, can significantly improve the ductility of polycrystalline Ni_3Al.[3] At room temperature, the addition of only 0.05 wt % ($\approx$0.25 at. %) of boron increases the elongation of polycrystalline Ni_3Al from a few percent to values of 45–50 %.[5] This effect, however, is only observed in specimens that contain excess Ni. Because boron is known to segregate preferentially toward grain boundaries, one explanation for its dramatic effect on ductility is that it promotes better cohesion across the grain boundary plane.[6–11] More recent experiments have shown that boron also improves the ductility of single Ni_3Al crystals,[12] suggesting that a bulk effect should be considered in addition to the grain boundary strengthening effect of boron when explaining the improvement in ductility of polycrystalline Ni_3Al due to B additions.

While the *intrinsic* factors, such as poor grain boundary cohesion, are important, in many cases dominant, in limiting ductility, recent work by George, Liu, and Pope has shown[13] that *extrinsic* factors, in particular the humidity, can be a major cause of low ductility in some systems. Their results demonstrate that the poor ductility commonly observed in air tests involves the dissociation of H_2O to generate atomic hydrogen, which diffuses into the region of the crack tip and promotes brittle crack propagation. George, Liu, and Pope[13] have suggested that the principal role of boron in ductlizing Ni_3Al is to suppress the environmental embrittlement.

The purpose of the work reported here is to understand the electronic mechanism underlying the contrasting effects of the boron-induced strengthening and the hydrogen-induced embrittlement in Ni_3Al. To this end, we have carried out full-potential linear-muffin-tin-orbital (FLMTO) total-energy calculations to investigate the effects of boron, hydrogen, and boron-hydrogen impurities on the electronic structure of Ni_3Al, and to study the changes and trends of bonding associated with these impurities. Our underlying assumption is that changes in the electronic structure produced when either or both of

these solutes is introduced into interstitial sites in the perfect lattice will be qualitatively similar to the changes induced when they occupy similar, but more open sites at grain boundaries. Although there have been some limited theoretical studies of boron in Ni_3Al,[14] the calculations reported here are, to our knowledge, the first of hydrogen and hydrogen-boron together in Ni_3Al.

In Sec. II, we briefly describe the FLMTO method and discuss the supercell geometry used in the impurity calculations. In Sec. III A, we describe the numerical results of the pure Ni_3Al system and compare them with previous calculations. These results will be used as a reference for comparison with the changes in the electronic structure induced by the boron and/or hydrogen impurities in the following sections. The results of the changes in the electronic structure induced by boron, hydrogen, and boron and hydrogen together in Ni_3Al are presented in Secs. III B, III C, and III D, respectively. In order to study the effect of the local environment of the impurity on the electronic structure, we have performed *ab initio* supercell calculations with impurities at two different octahedral sites: (a) an octahedral Ni-rich site (a site having six Ni nearest neighbors), and (b) an octahedral Ni-deficient site (a site having four Ni and two Al nearest neighbors). Results will be presented for the total energies, the site- and l-projected densities of states, and the impurity-induced charge densities for various impurity configurations. Finally, in Sec. IV a brief summary and statement of conclusions are presented.

II. COMPUTATIONAL METHOD

Our method of solving the electronic structure problem is based on the full-potential linear-muffin-tin-orbital (FLMTO) method, which includes the nonspherical terms within the muffin-tin spheres. These calculations differ from the more common LMTO calculations based on the atomic sphere approximation (ASA),[15] in that there is a true interstitial region and the LMTO bases have, in general, a nonzero kinetic energy in the interstitial which is treated as a variational parameter.

The FLMTO method has been described in detail elsewhere.[16] For the exchange and correlation potential, a form due to Ceperley and Alder,[17] as parametrized by Perdew and Zunger,[18] is used. The electrostatic potential is found using the method of Weinert.[19] The input and output potentials are then mixed using Broyden's mixing scheme,[20] which we found to give quick convergence to self-consistency. Spherical harmonic expansions for the muffin-tin potential and the charge density were carried out through $l=12$. A reciprocal-lattice vector cutoff of 6.0 is used. The representative points in the Brillouin zone are chosen according to the special points scheme.[21] Thirty special points were used in the irreducible $\frac{1}{16}$ portion of the Brillouin zone. The total and l-projected densities of states were calculated on a tetrahedral mesh,[22] using 120 points in the irreducible portion of the Brillouin zone.

The supercell employed in our calculations, shown in Fig. 1, consists of six atomic layers in the [001] direction and two layers in both the [100] and [001] directions.

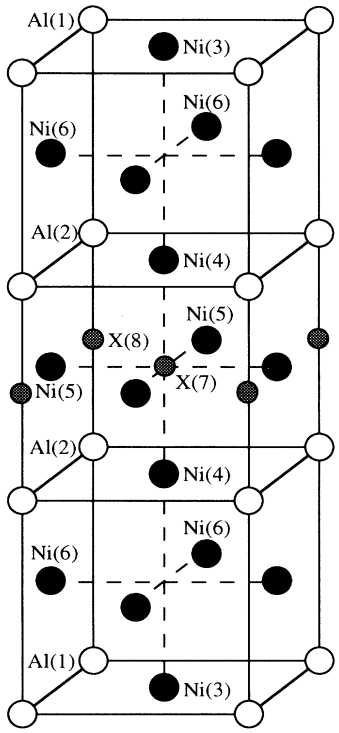

FIG. 1. Supercell geometry used in the calculation. The filled, empty, and gray shaded circles represent Ni, Al, and X atoms, respectively (X stands for the boron or hydrogen impurity). The two types of octahedral sites for the impurity are denoted by $X(7)$ and $X(8)$, respectively.

Inequivalent atoms in the cell are denoted by numerical labels (enclosed in parentheses), depending on their point-group symmetry. For example, Al atoms at (0,0,0) and (0,0,1) have a D_{4h} and a C_{4v} point-group symmetry, and are referred to as Al(1) and Al(2) atoms, respectively. Based on x-ray-diffraction intensity ratios, Masahashi, Takasugi, and Izumi[23] conclude that boron occupies octahedral interstices in the Ni_3Al structure. Therefore, in order to study the effect of the local environment of the impurity on the electronic structure, the impurity (labeled by X) was placed at two different octahedral interstitial sites:[23] (1) at the center of the octahedral cell [$X(7)$], where the impurity has four Ni(5) and two Ni(4) nearest neighbors, and (2) at the center of the cube edge [$X(8)$], where the impurity has four Ni(5) and two Al(2) nearest neighbors. We will refer to the $X(7)$ and $X(8)$ sites as Ni-rich and Ni-deficient octahedral sites (O sites), respectively. Thus we model the absorbed impurity in a supercell geometry with the periodicity of AlNi-Ni-AlNi-NiX-AlNi-Ni layers stacking along the [001] direction. Such an arrangement corresponds to an impurity concentration of 8.3 at. % when one of the octahedral sites is occupied. In all calculations, atomic relaxation was ignored and the lattice constant was kept frozen at the value of 3.568 Å for pure Ni_3Al.[24,25] Muffin-tin radii of 1.07 Å were chosen to be equal for both Ni and Al atoms. The muffin-tin radii for the boron and hydrogen impurity were chosen also to be equal at 0.71 Å.

III. NUMERICAL RESULTS AND DISCUSSION

A. Electronic structure of Ni_3Al

Though the total charge density can reveal the distribution of the interstitial and core charge, interesting details of microscopic charge transfer and the formation of a directional bond due to Ni-d/Al-p hybridization can be described better by plotting the bonding-charge density $\Delta\rho(\mathbf{r})$. The bonding charge density is defined as the difference between the total charge density in the solid and the superpositions of neutral atomic charge densities placed at atomic sites, i.e.,

$$\Delta\rho(\mathbf{r})=\rho_{\text{solid}}(\mathbf{r})-\sum_{\alpha}\rho_{\alpha}(\mathbf{r}-\mathbf{r}_{\alpha})\ . \tag{1}$$

Therefore, the bonding-charge density represents the net charge redistribution as atoms are brought together to form the crystal.

The bonding-charge density on the (110) plane is plotted in Fig. 2 in units of 10^{-3} e/(a.u.)^3. Here solid and dotted curves represent contours of increased (accumulation) and decreased (depletion) electronic charge densities. We find that the depletion of electron density at the aluminum sites is accompanied by significant *anisotropic* buildup of the directional d-bonding charge at the nickel sites. The bonding charge accumulation at the Ni site is along the nearest-neighbor (NN) Ni-Al and next-nearest-neighbor (NNN) Ni-Ni directions. The bonding directionality is caused mainly by the polarization of p electrons at the Al sites as a result of the p-d hybridization effect. One can also see a significant buildup of the interstitial bonding charge at the octahedral sites (sites between NNN Ni atoms and NNN Al atoms) between the (001) Ni-Al planes. These results are in qualitative agreement with those of recent warped-muffin-tin LMTO electronic structure calculations.[26] However, it is *the nonspherical corrections* to the spherical potential, absent in our warped LMTO calculations, that yield the directionality of the d-bonding charge at the Ni sites. Thus the bonding mechanism in Ni_3Al involves the combination of charge transfer and strong Al-p/Ni-d hybridization effects. This is one of the most remarkable features of intermetallics.

The bonding-charge density on the (001) and (002) planes is shown in Figs. 3 and 4, respectively. The (001) plane contains both Al and Ni atoms, while the (002) plane contains solely Ni atoms. The bonding charge on the (001) plane is mainly due to the Al/p-Ni/d hybridization, and that on the (002) plane is due to Ni/d-Ni/d hybridization. It can be seen that the bonding between the NN Al and Ni atoms on the (001) plane is mostly ionic in nature; charge is transferred from Al to Ni, which is in accord with the Pauling electronegativity difference. On the (002) plane, the d-d hybridization between the NN Ni atoms results in a charge difference which shows a $dd\pi$ bonding character. The presence of interstitial charge at the octahedral sites on these planes enhances the bonding between the NNN Ni atoms. The total charge in the aluminum and nickel muffin-tin spheres is 0.988 and 8.464 electrons, respectively. Because there are 10 ($3d^8$,$4s^2$) and 3 ($3s^2$,$3p^1$) valence electrons for the Ni and Al neutral atoms, each Al and Ni atom loses 2.012 and 1.536 electrons to the interstitial region. The partial s, p, and d muffin-tin charges are 0.261, 0.244, and 7.952

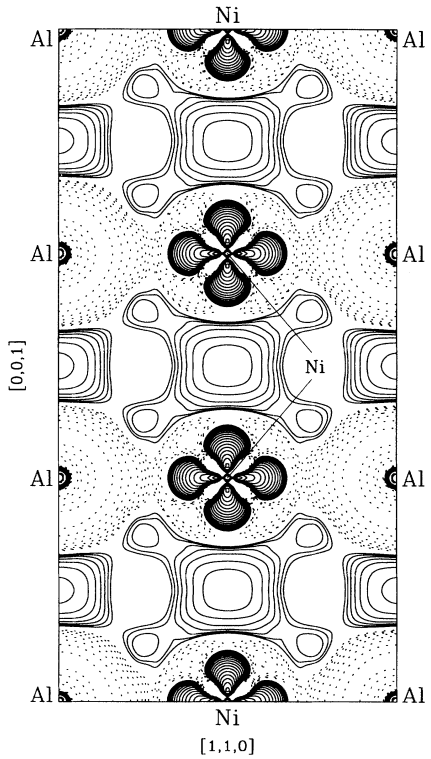

FIG. 2. The charge-density difference between Ni_3Al and the superposition of neutral Ni and Al atomic charge densities on the (110) planes. The solid (dotted) contours denote contours of increased (decreased) density as atoms are brought together to form the Ni_3Al crystal. Contours start from $\pm 8.0\times10^{-4}$ e/(a.u.)^3 and increase successively by a factor of root 2.

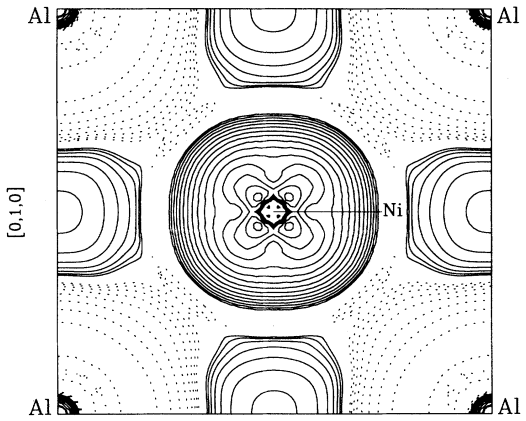

FIG. 3. Bonding charge density of Ni_3Al on the (001) plane. Solid (dotted) contours denote contours of increased (decreased) charge density. Contours start from $\pm 8.0\times10^{-4}$ e/(a.u.)^3, and increase successively by a factor of root 2.

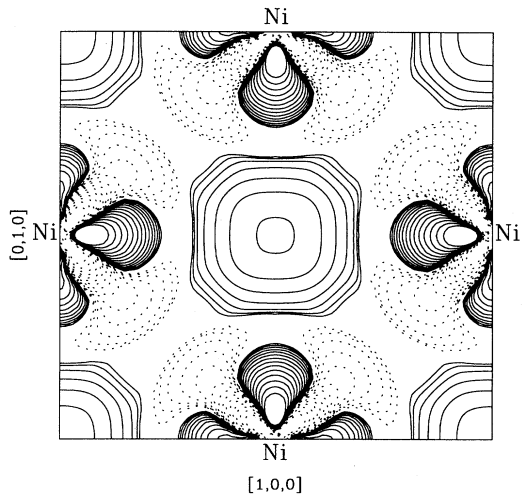

FIG. 4. Bonding charge density of Ni_3Al on the (002) plane. Solid (dotted) contours represent contours of increased (decreased) charge density. Contours starts from $\pm 1.0\times 10^{-3}$ e/(a.u.)^3 and increase successively by a factor of root 2.

electrons for the Ni atom and 0.412, 0.462, and 0.104 electrons for the Al atom.

In Fig. 5 we show the total density of states (DOS) and the partial density of states for the Ni d-derived and Al p-derived bands for the pure system (solid curves). The density of states agrees well with the existing calculations.[27] Besides the strong Ni d-d bonding, it can clearly be seen that a characteristic feature of the density of states in Ni_3Al is the hybridization between Ni d and Al p states. As shown in Fig. 5, a sharp bonding peak and antibonding peak is located near -0.25 and 0.1 Ry, respectively. Another feature of the electronic structure for Ni_3Al in the $L1_2$ structure is a valley located at about 0.05 Ry above the Fermi energy, which separates the p-d bonding and antibonding states. The calculated density of states at the Fermi energy, $N(E_F)$, is 81.60 states/(Ry cell). This is in good agreement with the value of 82.81 states/(Ry cell) obtained by Nautiyal and Auluck,[27] is between the values of 75.2 states/(Ry cell) obtained by Min, Freeman, and Jansen[28] and 85.6 obtained by Wosicki and Jezierski,[29] and is higher than the value of 70.5 states/(Ry cell) obtained by Hackenbracht and Kubler.[30] However, though all the theoretical calculations agree reasonably well with each other, they differ substantially from the experimental value of 174.6 states/(Ry cell) obtained by Buis, Franse, and Brommer,[31] and of 150 states/(Ry cell) obtained by Dood and Chatel.[32]

B. Effect of boron in Ni_3Al

In this section we consider the electronic mechanism underlying the enhanced ductility induced by boron additions to Ni_3Al. In order to study the effect of the local environment of the impurity on the electronic structure, we consider two different types of octahedral sites $X(7)$ and $X(8)$ in Fig. 1. To compare the energetics of the different impurity configurations we have calculated the impurity formation energy

$$\Delta E_{\rm imp} = E_{\rm tot}(Ni_3AlX) - E_{\rm tot}(Ni_3Al) - E_{\rm tot}(X) \ . \quad (2)$$

Here $E_{\rm tot}(Ni_3AlX)$ is the total energy of the supercell with the impurity X placed at a certain octahedral site, $E_{\rm tot}(Ni_3Al)$ is the total energy of the supercell without the impurity, and $E_{\rm tot}(X)$ is the total energy of an isolated impurity atom. We find that the impurity formation energies for a boron impurity placed at the Ni-rich $[X(7)]$ and Ni-deficient $[X(8)]$ octahedral sites in Ni_3Al are -4.4 eV/(unit cell) and -0.08 eV/(unit cell), respectively. Thus boron prefers to occupy octahedral sites which are surrounded by nearest-neighbor Ni sites. (These calculations were done at the experimental lattice constant, $a = 3.568$ Å.)

It is instructive to compare the total valence charge in each inequivalent muffin-tin (MT) sphere and in the interstitial for the supercell in which the boron impurity occupies the Ni-rich octahedral site and for the pure Ni_3Al system. Values of the integrated MT and interstitial charge for each inequivalent MT sphere for the two systems are summarized in Table I. Also listed in this table are values of the difference of MT charge, Δq, between the $Ni_3AlB_{1/3}$ and Ni_3Al systems, namely the charge

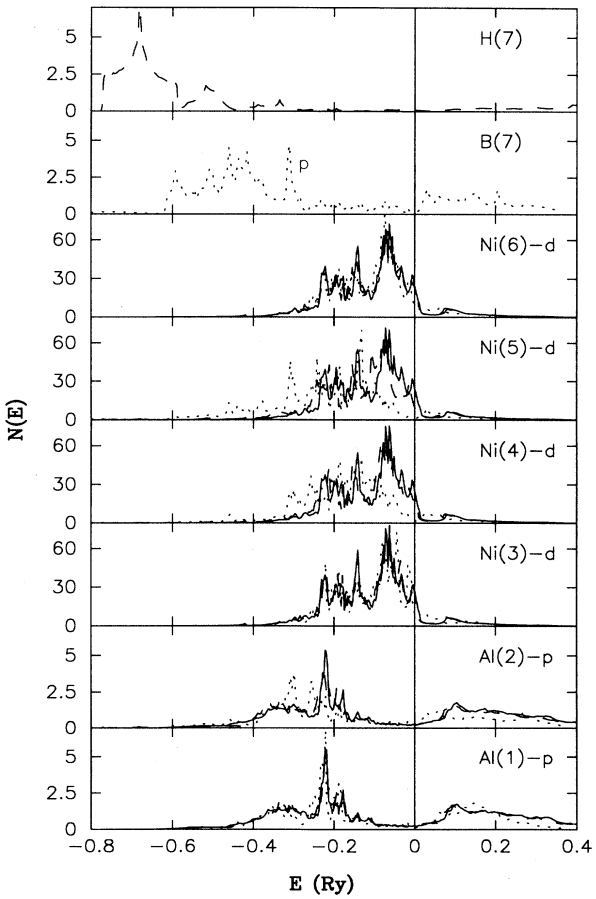

FIG. 5. The site- and l-projected DOS's of Ni_3Al (solid curves), $Ni_3AlB_{1/3}$ (dotted curves), and $Ni_3AlH_{1/3}$ (dashed curves) in units of states/Ry-unit cell. For boron the B-p-derived band is plotted, and for hydrogen the H-s-derived band.

TABLE I. Total integrated muffin-tin and interstitial charges for $Ni_3AlB_{1/3}$ (B in the Ni-rich O site) and for pure Ni_3Al. N_i denotes the number of atoms of each muffin-tin type in the supercell. The last column (except for the last two rows) is the difference of MT charge in the preceding two columns, i.e., $\Delta q = q(Ni_3AlB_{1/3}) - q(Ni_3Al)$. The Δq in the last two rows is the change in the total MT and interstitial charge, namely $\Delta q_{MT} = q_{MT}(Ni_3AlB_{1/3}) - q_{MT}(Ni_3Al) - q_{MT}(B_{1/3})$ and $\Delta q_{int} = q_{int}(Ni_3AlB_{1/3}) - q_{int}(Ni_3Al) - [q_{valence}(B_{1/3}) - q_{MT}(B_{1/3})]$, where $q_{valence}(B_{1/3})$ is the total valence charge of a boron atom and $q_{MT}(B_{1/3})$ is the MT charge of boron in the supercell.

Name	Type	N_i	$q(Ni_3AlB_{1/3})$	$q(Ni_3Al)$	Δq
Al	1	1	0.969	0.988	−0.019
Al	2	2	0.951	0.988	−0.037
Ni	3	1	8.451	8.464	−0.013
Ni	4	2	8.611	8.464	0.147
Ni	5	2	8.780	8.464	0.316
Ni	6	4	8.444	8.464	−0.020
B	7	1	1.293		
MT total			81.17	79.14	0.737
interstitial total			20.83	19.86	−0.737

transfer for each MT sphere due to the presence of boron. We find that the presence of boron induces a charge accumulation in the nearest-neighbor nickel sites [Ni(4) and Ni(5)], and induces a charge depletion in the Al(1) and Al(2) sites and the more distant Ni(3) and Ni(6) sites. Though the charge transfer does not offer detailed information on the spatial distribution and directionality of bonding charge, it does show which atomic sites gain or lose additional bonding charge. It is also instructive to compare the total MT charge accumulation (depletion), $\Delta q_{MT} = \sum_i \Delta q^i_{MT} N_i$, where Δq^i_{MT} is the charge accumulation (depletion) in the MT sphere of type i, and N_i is the number of atoms of type i in the supercell. For each type, values of Δq^i_{MT} and N_i are also listed in Table I. The total charge depleted from the MT spheres is 0.186 electrons, which is too small to account for the charge of 0.926 electrons accumulated in the MT spheres. Thus most of the charge accumulated in the MT spheres is due to charge transfer from the interstitial.

To understand the effect of absorbed boron on the bonding properties of Ni_3Al, we next consider the redistribution of charge induced by the impurity atom when placed at the Ni-rich octahedral site [$X(7)$]. This can be best described by the *difference of bonding charge density* between $Ni_3AlB_{1/3}$ and Ni_3Al, namely

$$\Delta\rho_{ind}(\mathbf{r}) = \Delta\rho_{solid}(Ni_3AlX) - \Delta\rho_{solid}(Ni_3Al)$$
$$= \rho_{solid}(Ni_3AlX) - \rho_{solid}(Ni_3Al) - \rho_{atom}(X) \ . \quad (3)$$

We will refer to $\Delta\rho_{ind}(\mathbf{r})$ as the impurity-induced charge density. The impurity-induced charge density on the (110) and (002) planes is shown in Figs. 6 and 7, respectively. One can see that the enhancement of bonding charge around the Ni(4) site in Fig. 6 is quite asymmetric relative to the (001) plane through the atom. This is expected because the presence of boron breaks such a mirror symmetry. Though boron induces a decrease of the

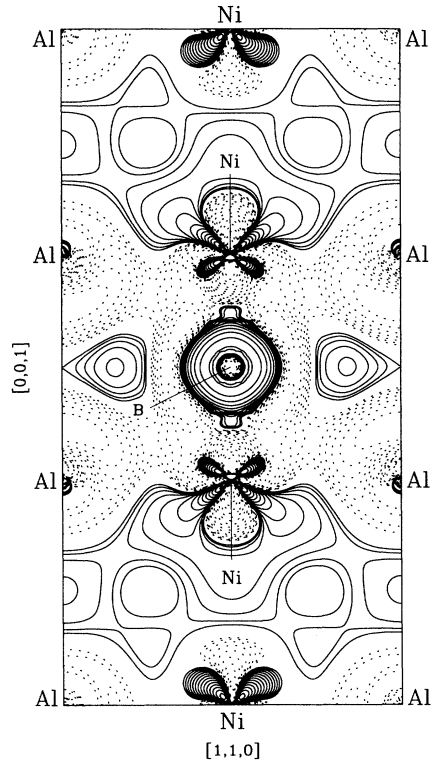

FIG. 6. Boron-induced charge density of $Ni_3AlB_{1/3}$ on the (110) plane. Boron occupies the Ni-rich octahedral site [$X(7)$]. Solid (dotted) contours denote positive (negative) induced charge density. Contours start from $\pm 4.0\times10^{-4}$ e/(a.u.)^3 and increase successively by a factor of root 2.

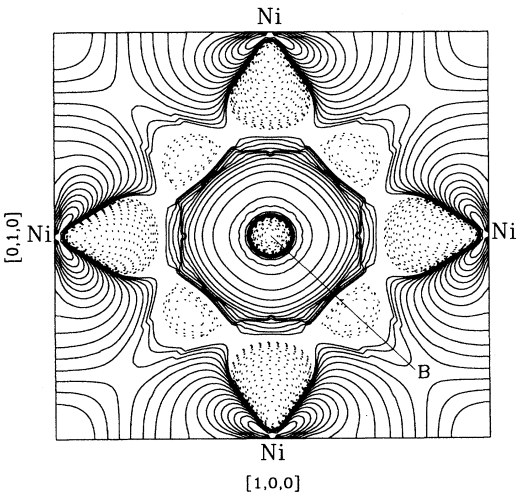

FIG. 7. Boron-induced charge density of $Ni_3AlB_{1/3}$ on the (002) plane. Boron occupies the Ni-rich octahedral interstitial site [$X(7)$]. Solid (dotted) contours represent positive (negative) induced charge density. Contours start from $\pm 8.0\times10^{-4}$ e/(a.u.)^3 and increase successively by a factor of root 2.

total MT valence charge in the Ni(3) site (Table I), the redistribution of the bonding charge about the Ni(3) site is significant. A comparison of Figs. 2 and 6 shows that boron induces a charge accumulation about Ni(3) in a direction where there is a depletion of the bonding charge $\rho_{\text{solid}}(Ni_3Al)$ in the pure Ni_3Al system. Thus the bonding-charge directionality, $\Delta\rho_{\text{solid}}(Ni_3AlX)$, of Ni(3) is *reduced* due to the presence of a small percentage of boron. More importantly, boron causes a significant buildup of interstitial charge near the (001) planes containing solely Ni atoms [Ni(6) atoms], which in turn enhances both the intraplanar bonding between the NN Ni(6) atoms and the interplanar bonding between the NNN Al(1) and Al(2) atoms and the NNN Ni(3) and Ni(4) atoms. Note that boron also induces an additional charge depletion from all Al atoms. The boron-induced charge density on the (002) plane is shown in Fig. 7. Boron induces a substantial enhancement of interstitial bonding charge between the NN Ni(5) sites, thus increasing the intraplanar Ni—Ni bonding within the (002) planes. Finally, an interesting point to note is that electronic charge is depleted from the interstitial regions near the NiB plane in the [001] direction. This suggests a weaker local cohesion near these planes. This may be due to the fact that the local concentration of boron is high enough in our calculations (8.3 at. %) so as to weaken the local cohesion. This is consistent with the experimental results that Ni_3Al single crystals show a reduced ductility when doped with more than 0.8 at. % boron.[12]

The *l*- and site-projected DOS of $Ni_3AlB_{1/3}$ (dotted lines) are also shown in Fig. 5, and they can be compared with those of Ni_3Al (solid lines). One can see that the effect of boron on the electronic structure is *local,* in that the boron affects primarily only its nearest-neighbor nickel and aluminum atoms [Ni(4), Ni(5), and Al(2)]. The density of states show that there is strong hybridization between the B-*p* and primarily Ni(4)- and Ni(5)-*d* states. The downward shift (of about 0.06 Ry) in the Ni(4) and Ni(5) *d*-projected density of states is consistent with the calculated MT charge transfer of these atoms. The large broadening of the Ni(5)-*d* and Ni(4)-*d* DOS's is due to the Ni-*d* and B-*p* hybridizations. Compared to the DOS of Ni_3Al, the Fermi energy is shifted up in the valley which separates the bonding and antibonding energy regions.

C. Effect of H in Ni_3Al

In this section, we consider the electronic mechanism underlying the hydrogen-induced embrittlement in Ni_3Al. We model the absorbed hydrogen in the supercell geometry of Fig. 1. The hydrogen formation energy is found to be -3.85 eV/(unit cell) and -2.60 eV/(unit cell) for placing the hydrogen impurity at the $X(7)$ (Ni-rich) and $X(8)$ (Ni-deficient) octahedral sites, respectively, indicating that hydrogen also prefers to occupy Ni-rich octahedral sites. The difference in energy for H in the two different octahedral sites is mainly due to H-Al interaction, which is only present in one case. We found that the H-Al interaction leads to some charge transfer to Al, which results in lowered band energy but increased electrostatic energy. The net result is the increased total energy for H in the Ni-deficient octahedral site.

In Table II we list values for the integrated valence MT and interstitial charge for the $Ni_3AlH_{1/3}$ supercell where the hydrogen occupies the Ni-rich octahedral site, and for the pure Ni_3Al system. The additional charge transfer induced by H is significant only for the Ni(4) and Ni(5) atoms at the apexes of the octahedron. As in the case of boron, the hydrogen-induced charge depletion from the Al, Ni(3), and Ni(6) sites is too small to account for the charge accumulation within the Ni(4) and Ni(5) MT spheres. Thus most of the charge accumulated within the Ni(4) and Ni(5) MT spheres arises from charge transfer from the interstitial.

Figures 8 and 9 show the impurity-induced charge on the (110) and (002) planes for $Ni_3AlH_{1/3}$. To compare with the boron-induced charge redistribution in Figs. 6 and 7, we use the same contour levels for both $Ni_3AlH_{1/3}$ and $Ni_3AlB_{1/3}$. It is clear that hydrogen induces a much weaker charge redistribution than boron. More importantly, the enhancement of interstitial bonding charge, found near the pure Ni(6) plane in the [001] direction for the case of boron, is completely missing in the case of hydrogen. Thus hydrogen does not provide the intraplanar and interplanar bonding enhancements found in the boron-doped system. Furthermore, hydrogen affects the more distant nickel atoms [Ni(3)] quite differently. Significantly, hydrogen induces a buildup of charge along the [001] direction, and a charge depletion within the (001) planes containing equal numbers of Ni(3) and Al atoms. This charge redistribution results in an *enhancement* of the *bonding-charge* directionality of Ni(3), which could be interpreted as the signature of a brittle system. Also note that hydrogen causes a larger redistribution of charge on the Ni(3) than on the Al(2) sites, a rather surprising result in view of the larger distance of the Ni(3) atoms from the hydrogen impurity. Hydrogen

TABLE II. Total integrated muffin-tin and interstitial charge for $Ni_3AlH_{1/3}$ (H in the Ni-rich *O* site) and for pure Ni_3Al. N_i denotes the number of atoms of each muffin-tin type in the supercell. The last column (except for the last two rows) is the difference of MT charge in the preceding two columns, i.e., $\Delta q = q(Ni_3AlH_{1/3}) - q(Ni_3Al)$. The Δq in the last two rows denotes the change in the total MT and interstitial charge, namely $\Delta q_{MT} = q_{MT}(Ni_3AlH_{1/3}) - q_{MT}(Ni_3Al) - q_{MT}(H_{1/3})$ and $\Delta q_{int} = q_{int}(Ni_3AlH_{1/3}) - q_{int}(Ni_3Al) - [q_{valence}(H_{1/3}) - q_{MT}(H_{1/3})]$, where $q_{valence}(H_{1/3})$ is the total valence charge of a hydrogen atom, and $q_{MT}(H_{1/3})$ is the MT charge of hydrogen in the supercell.

Name	Type	N_i	$q(Ni_3AlH_{1/3})$	$q(Ni_3Al)$	Δq
Al	1	1	0.985	0.988	−0.003
Al	2	2	0.984	0.988	−0.004
Ni	3	1	8.462	8.464	−0.002
Ni	4	2	8.516	8.464	0.052
Ni	5	2	8.570	8.464	0.106
Ni	6	4	8.461	8.464	−0.003
H	7	1	0.817		
MT total			80.25	79.14	0.293
interstitial total			19.75	19.86	−0.293

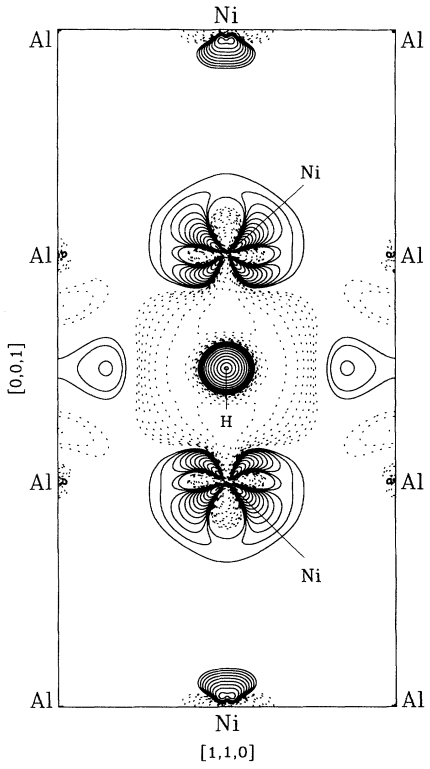

FIG. 8. Hydrogen-induced charge density of $Ni_3AlH_{1/3}$ on the (110) plane. Hydrogen occupies the Ni-rich octahedral interstitial site [$X(7)$]. Solid (dotted) contours represent positive (negative) induced charge density. Contours start from $\pm 4.0\times 10^{-4}$ e/(a.u.)^3 and increase successively by a factor of root 2.

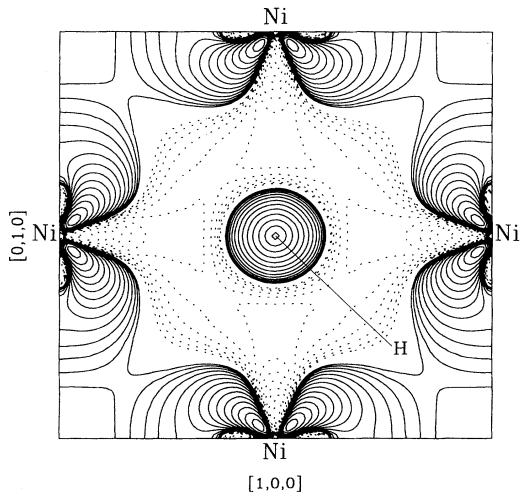

FIG. 9. Hydrogen-induced charge density of $Ni_3AlH_{1/3}$ on the (002) plane. Hydrogen occupies the Ni-rich octahedral interstitial site [$X(7)$]. Solid (dotted) contours represent positive (negative) induced charge density. Contours start from $\pm 8.0\times 10^{-4}$ e/(a.u.)^3 and increase successively by a factor of root 2.

causes a charge redistribution within the (002) plane (Fig. 9) similar to that induced by boron, which, however, is quantitatively weaker. Overall, while we cannot conclude directly that such a charge redistribution implies brittleness, a comparison of Figs. 6, 7, 8, and 9 does suggest that hydrogen decreases local crystal cohesion. This is certainly consistent with its role as an embrittling agent.

In order to gain insight at the microscopic level into the effect of H-s/Ni-d hybridization, in Fig. 5 we inspect the l- and site-projected DOS's for $Ni_3AlH_{1/3}$ (dashed lines), and compare them with those of Ni_3Al (solid lines) and $Ni_3AlB_{1/3}$ (dotted curves). It is clearly seen in Fig. 5 that the hybridization induced by hydrogen is much weaker than that induced by boron, because there is very little overlap between H-s and Ni-d and H-s and Al-p states over the whole energy spectrum. The changes in the DOS induced by H are very small for all atoms except for the nearest-neighbor Ni(5) atoms which are on the (001) NiH plane. Note that there is a small downward shift in the Ni(5)-d band by about 0.02 Ry, which is consistent with the charge transfer to the Ni(5) sites listed in Table II.

D. Effect of B and H in Ni_3Al

In this section we consider the effect of both boron and hydrogen impurities on the electronic structure of Ni_3Al. We have considered two impurity configurations: (1) boron and hydrogen occupying the $X(7)$ (Ni-rich) and $X(8)$ (Ni-deficient) sites in the supercell in Fig. 1, respectively; and (2) boron and hydrogen occupying the $X(8)$ and $X(7)$ sites, respectively. The impurity formation energies for these two configurations are -6.33 and -3.55 eV, respectively, indicating that even in the presence of hydrogen impurities boron prefers to occupy the $X(7)$ octahedral Ni-rich sites, which maximize the B-p and Ni-d hybridizations. In the rest of this section, we will consider only the first impurity configuration, which has the lower formation energy, and compare this system with those discussed in Secs. III A–III C.

The calculated MT and interstitial charge for $Ni_3AlB_{1/3}H_{1/3}$ and Ni_3Al are summarized in Table III. It is instructive to compare the values of the induced charge transfer with those found for the $Ni_3AlB_{1/3}$ system shown in Table I. One can see that the presence of hydrogen yields a weaker depletion of electron charge on the Al(2) sites, and a stronger charge accumulation on the Ni(5) sites. Note that both these two types of sites are nearest neighbors to the hydrogen impurity. There is very little change in the charge of the other, more distant, MT spheres, indicating that the effect of hydrogen is local.

To further explore the bonding character, we show the impurity-induced charge density on the (110) and (002) planes in Figs. 10 and 11, respectively. The changes induced by H are quite localized near the hydrogen atom. Comparison with Fig. 6 confirms that the local charge depletion around the Al(2) atoms is weaker for the $Ni_3AlB_{1/3}H_{1/3}$ system. Furthermore, as for $Ni_3AlB_{1/3}$, the enhancement of interstitial charge near the pure Ni(6)

TABLE III. Total integrated muffin-tin and interstitial charges for $Ni_3AlB_{1/3}H_{1/3}$ (B in the Ni-rich O site) and for the pure Ni_3Al. N_i denotes the number of atoms of each muffin-tin type in the supercell. The last column is the difference of MT charges in the preceding two columns, i.e., $\Delta q = q(Ni_3AlB_{1/3}H_{1/3}) - q(Ni_3Al)$. The Δq in the last two rows is the change in the total MT and interstitial charge, i.e., $\Delta q_{MT} = q_{MT}(Ni_3AlB_{1/3}H_{1/3}) - q_{MT}(Ni_3Al) - q_{MT}(B_{1/3}) - q_{MT}(H_{1/3})$ and $\Delta q_{int} = q_{int}(Ni_3AlB_{1/3}H_{1/3}) - q_{int}(Ni_3Al) - [q_{valence}(B_{1/3}) - q_{MT}(B_{1/3})] - [q_{valence}(H_{1/3}) - q_{MT}(H_{1/3})]$. Here, $q_{valence}(B_{1/3})$ and $q_{valence}(H_{1/3})$ are the total valence charges of a boron and a hydrogen atom, and $q_{MT}(B_{1/3})$ and $q_{MT}(H_{1/3})$ are the MT charges of boron and hydrogen in the supercell.

Name	Type	N_i	$q(Ni_3AlB_{1/3}H_{1/3})$	$q(Ni_3Al)$	Δq
Al	1	1	0.967	0.988	−0.021
Al	2	2	0.991	0.988	−0.003
Ni	3	1	8.451	8.464	−0.013
Ni	4	2	8.610	8.464	0.146
Ni	5	2	8.875	8.464	0.411
Ni	6	4	8.439	8.464	−0.025
B	7	1	1.294		
H	8	1	0.852		
MT total			82.27	79.14	0.984
interstitial total			20.73	19.86	−0.984

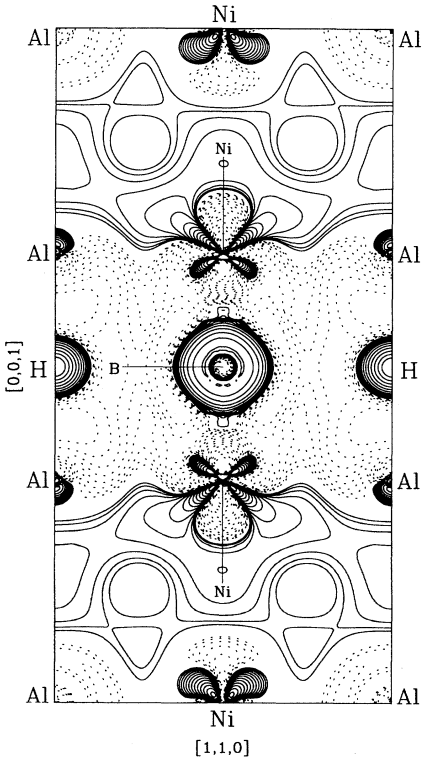

FIG. 10. Impurity-induced charge density of $Ni_3AlB_{1/3}H_{1/3}$ on the (110) plane. The boron and hydrogen impurities occupy the $X(7)$ and $X(8)$ sites in Fig. 1, respectively. Solid (dotted) contours represent positive (negative) induced charge density. Contours start from $\pm 4.0\times10^{-4}$ e/(a.u.)^3 and increase successively by a factor of root 2.

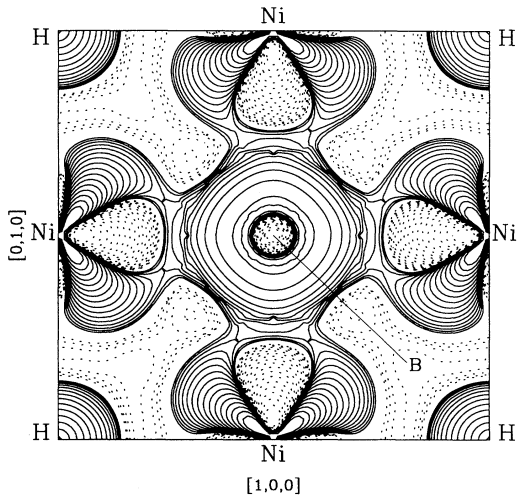

FIG. 11. Impurity-induced charge density of $Ni_3AlB_{1/3}H_{1/3}$ on the (002) plane. The boron and hydrogen impurities occupy the $X(7)$ and $X(8)$ sites in Fig. 1, respectively. Solid (dotted) contours represent positive (negative) induced charge density. Contours start from $\pm 8.0\times10^{-4}$ e/(a.u.)^3 and increase successively by a factor of root 2.

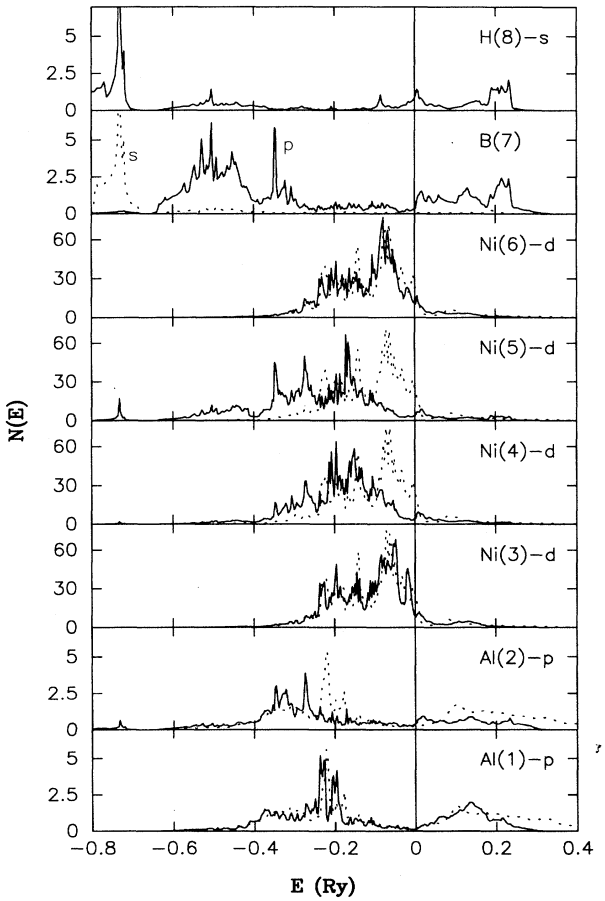

FIG. 12. Comparison of the site- and l-projected DOS's of $Ni_3AlB_{1/3}H_{1/3}$ (solid curves) with those of pure Ni_3Al (dotted curves). For boron, the s (dotted curves) and p- (solid) derived bands are shown. For hydrogen the H-s-derived bands are shown.

plane and the reduction of the bonding-charge directionality around the Ni(3) atoms remain the most dominant features of the bonding behavior of the system. Additional changes in bonding-charge density induced by H are quantitative rather than qualitative when compared with those for $Ni_3AlB_{1/3}$, and we conclude that bonding in $Ni_3AlB_{1/3}H_{1/3}$ is similar to $Ni_3AlB_{1/3}$.

The site- and *l*-projected DOS's for $Ni_3AlB_{1/3}H_{1/3}$ (solid lines) are shown in Fig. 12, and compared with those of Ni_3Al (dotted lines). Comparison with the corresponding DOS for the $Ni_3AlB_{1/3}$ system in Fig. 5 shows that there is a downward shift of the Ni(5)-*d* band, confirming the extra charge transfer to the Ni(5) atoms in Table III. Both the Ni(5)-*d*- and Al(2)-*p*-derived bands exhibit additional peaks at -0.73 Ry below the Fermi energy, resulting from the hybridization between the Ni(5)-*d* and H(8)-*s* and Al(2)-*p* and H(8)-*s* states, respectively. Overall, our calculations show that the changes in the electronic structure and bonding induced by hydrogen in Ni_3Al are small relative to those induced by boron.

IV. CONCLUSION

We have studied the effect of boron and hydrogen impurities on the bonding charge in Ni_3Al employing first-principles electronic structure calculations based on the FLMTO method. We have calculated the energetics and site- and *l*-projected densities of states, and the impurity-induced charge density for various impurity configurations, to study the effect of the local environment of the impurity on the electronic structure. We find that changes in the electronic structure induced by boron result from the hybridization of the *d* states of the nearest-neighbor Ni atoms with adjacent B-*p* states. Thus boron prefers to occupy Ni-rich octahedral interstices [$X(7)$]. Boron is found to enhance greatly the intraplanar metallic bonding between the Ni atoms, to enhance the interplanar bonding between the NiAl layers in the [001] direction, and to reduce the bonding-charge directionality near the Ni(3) atoms. Thus we conclude that in such an environment boron acts to increase the cohesion of the crystal. In contrast, hydrogen is found to enhance the bonding-charge directionality near the Ni(3) atoms, and provides virtually no interstitial charge enhancement. This suggests that hydrogen does not promote local cohesion. When both boron and hydrogen are present in the system, the dominant changes in the electronic structure (DOS, induced charge densities) are induced by boron, and hydrogen seems to have very little effect. Overall, we find that our calculations are in qualitative accord with the known behavior of boron and hydrogen in Ni_3Al, and they suggest that the origin of the remarkable effects of these solutes may lie primarily in the fundamental changes they induce in the electronic structure of this material.

ACKNOWLEDGMENTS

The research at California State University Northridge (CSUN) was supported through the U.S. Army Research Office under Grant No. DAAH04-93-G-0427, the Lawrence Livermore National Laboratory through Grant No. B157318, and the Office of Research and Sponsored Projects at CSUN. The research at Lawrence Livermore National Laboratory was supported through the U.S. Department of Energy under Contract No. W-7405-ENG-48. We have benefitted greatly from discussions with Ruqian Wu.

[1]J. H. Westbrook, in *Ordered Alloys, Physical Metallurgy, and Structural Applications,* edited by B. H. Keaar, C. T. Sims, N. S. Stoloff, and J. H. Westbrook (Claitor's, Baton Rouge, LA, 1970), p. 1.

[2]C. T. Liu, in *Alloy Phase Stability,* edited by A. Gonis and G. M. Stocks (Kluwer, Amsterdam, 1989), p. 7.

[3]K. Aoki and O. Izumi, J. Jpn. Inst. Metals **43**, 1190 (1970).

[4]K. Aoki and O. Izumi, Acta Metall. **27**, 807 (1979).

[5]C. T. Liu, C. L. White, and J. A. Horton, Acta Metall. **33**, 213 (1985).

[6]C. T. Liu, C. L. White, C. C. Koch, and E. H. Lee, in *High Temperature Materials Chemistry II,* edited by L. A. Minir and D. Cubicciotti (Electrochemical Society, Remington, NJ, 1983), Vol. 83, p. 32.

[7]C. L. White, R. A. Padgett, C. T. Liu, and S. M. Yalisove, Scr. Metall. **18**, 1417 (1984).

[8]C. T. Liu and C. L. White, Scr. Metall. **35**, 643 (1987).

[9]G. S. Painter and F. W. Averil, Phys. Rev. Lett. **58**, 234 (1987).

[10]M. E. Eberhart and D. D. Vvedinsky, Phys. Rev. Lett. **58**, 61 (1987).

[11]S. P. Chen, A. F. Voter, and D. J. Srolovitz, in *High Temperature Ordered Intermetallic Alloys II,* edited by N. S. Stoloff, C. C. Koch, C. T. Liu, and O. Izumi, MRS Symposia Proceedings No. 8 (Materials Research Society, Pittsburgh, 1987), p. 45.

[12]F. E. Heredia and D. P. Pope, Acta Metall. Mater. **39**, 2017 (1991).

[13]E. P. George, C. T. Liu, and D. P. Pope, Scr. Metall. Mater. **27**, 365 (1992).

[14]C. L. Fu and M. H. Yoo, Mater. Chem. Phys. **32**, 25 (1992).

[15]O. K. Anderson, Phys. Rev. B **12**, 3060 (1975); H. L. Skriver, *The LMTO Method* (Springer, Berlin, 1984).

[16]David L. Price and Bernard R. Cooper, Phys. Rev. B **39**, 4945 (1989).

[17]D. M. Ceperley and B. J. Alder, Phys. Rev. Lett. **45**, 566 (1980).

[18]J. P. Perdew and A. Zunger, Phys. Rev. B **23**, 5048 (1981).

[19]M. Weinert, J. Math. Phys. **22**, 2433 (1981).

[20]G. P. Srivastara, J. Phys. A **17**, L317 (1984).

[21]D. J. Chadi and M. L. Cohen, Phys. Rev. B **8**, 5747 (1973).

[22]G. Gilat and N. R. Bharatiya, Phys. Rev. B **12**, 3497 (1975); L. T. Raubenheimer and G. Gilat, Phys. Rev. **157**, 586 (1967).

[23]N. Masahashi, T. Takasugi, and O. Izumi, Acta Metall. **36**, 1815 (1988).

[24]D. Hackenbracht and J. Kubler, J. Phys. F **13**, L179 (1983).

[25]*Smithells Metals Reference Book,* 6th ed., edited by E. A.

Brandes (Butterworths, London, 1983), pp. 6–14.
[26]N. Kioussis, H. Watanabe, R. G. Hemker, W. Gourdin, A. Gonis, and P. E. Johnson, in *Direct-Interface Interactions,* edited by E. P. Kvam, A. H. King, M. J. Mills, T. D. Sands, and V. Vitek, MRS Symposia Proceedings No. 319 (Materials Research Society, Pittsburgh, 1994), p. 363.
[27]T. Nautiyal and S. Auluch, Phys. Rev. B **45**, 13 930 (1992).
[28]B. I. Min, A. J. Freeman, and H. J. F. Jansen, Phys. Rev. B **37**, 6757 (1988).
[29]P. Wosicki and A. Jezierski, Physica B **161**, 172 (1989); D. Hackenbracht and J. Kubler, J. Phys. F **10**, 427 (1980).
[30]D. Hackenbracht and J. Kubler, J. Phys. F **10**, 427 (1980).
[31]N. Buis, J. J. M. Franse, and P. E. Brommer, Physica B&C **106**, 1 (1981).
[32]W. de Dood and P. F. Châtel, J. Phys. F **3**, 1039 (1973).